Robust Tracking of Migrating Cells Using Four-Color Level Set Segmentation*

Sumit K. Nath, Filiz Bunyak, and Kannappan Palaniappan

MCVL, Department of Computer Science, University of Missouri-Columbia, MO, USA
{naths, bunyak, palaniappank}@missouri.edu

Abstract. Understanding behavior of migrating cells is becoming an emerging research area with many important applications. Segmentation and tracking constitute vital steps of this research. In this paper, we present an automated cell segmentation and tracking system designed to study migration of cells imaged with a phase contrast microscope. For segmentation the system uses active contour level set methods with a novel extension that efficiently prevents false-merge problem. Tracking is done by resolving frame to frame correspondences between multiple cells using a multi-distance, multi-hypothesis algorithm. Cells that move into the field-of-view, arise from cell division or disappear due to apoptosis are reliably segmented and tracked by the system. Robust tracking of cells, imaged with a phase contrast microscope is a challenging problem due to difficulties in segmenting dense clusters of cells. As cells being imaged have vague borders, close neighboring cells may appear to merge. These false-merges lead to incorrect trajectories being generated during the tracking process. Current level-set based approaches to solve the false-merge problem require a unique level set per object (the N-level set paradigm). The proposed approach uses evidence from previous frames and graph coloring principles and solves the same problem with only four level sets for any arbitrary number of similar objects, like cells.

1 Introduction

Understanding behavior of migrating cells is becoming an emerging research area with many important applications. Behavior of migrating cells are important parameters of interest in understanding basic biological processes such as tissue repair , metastatic potential , chemotaxis , differentiation or analyzing the performance of drugs. Accurate segmentation and tracking of cells are vital steps in any cell behavior study.

In this paper, we present an automated cell segmentation and tracking system designed to study migration of cells imaged with a phase contrast microscope. Segmentation is performed using active contour level set methods with a novel extension that efficiently prevents false-merge problem. Tracking is done by resolving frame to frame correspondences between multiple cells using a multi-distance, multi-hypothesis algorithm. Cells that move into the field-of-view, arise from cell division or disappear due to apoptosis are reliably segmented and tracked by the system.

Simultaneous tracking of multiple cells imaged with a phase contrast microscope is a challenging problem due to difficulties in segmenting dense clusters of cells. As cells

* This work was supported by a U.S National Institute of Health NIBIB award R33 EB00573.

J. Blanc-Talon et al. (Eds.): ACIVS 2006, LNCS 4179, pp. 920–932, 2006.

being imaged have vague borders, close neighboring cells may appear to merge. These *false-merges* lead to incorrect trajectories being generated during the tracking process. Other challenges for tracking include high number of cells, non-linear motion, lack of discriminating features, mitosis (cell division), and fragmentation during segmentation. In [1], Chan and Vese presented an algorithm to automatically segment an image $I(\boldsymbol{y})$ into *two* distinct regions (or phases) by minimizing a minimal partition Mumford-Shah functional. A multiphase variant of the same algorithm was also proposed to handle 2^n unique phases [2]. However, as observed by Zhang *et al.,* [3], Dufour *et al.,* [4] and, Zimmer and Olivo-Marin [5], the two variants of the Chan and Vese algorithm are unsuitable for reliable cell segmentation due to the problem of apparent merges in cells.

Zhang *et al.,* proposed a $N-$ level set framework with an implicit coupling constraint to reliably segment cells in an image sequence [3]. While this alleviates the problem of apparent merging of cells, it is computationally expensive to implement. The approach we propose uses evidence from previous frames and graph coloring principles and solves the same problem with only four level sets for any arbitrary number of similar objects.

The organization of this paper is as follows. Section 2 describes the segmentation module. Salient features of our four-color level set segmentation algorithm are presented along with the related work, variants of the Chan and Vese level set algorithms and $N-$level set variant of Zhang *et al.,* algorithm [3]. Section 3 describes the tracking module. Comparative results and a discussion are presented in Section 4, while a conclusion is presented in Section 5.

2 Cell Segmentation Using Active Contour Level Set Methods

Accurate segmentation of individual cells is a crucial step in robust tracking of migrating cells as both over-segmentation (fragmentation) and under-segmentation (cell clumping) produce tracking errors (i.e., spurious or missing trajectories and, incorrect split and merge events). In this section, we describe three different level set segmentation methods and compare their performance for separating closely adjacent and touching cells in a dense population of migrating cells. The three techniques described in this section are all based on the "active contour without edges" energy functional with appropriate extensions, and include multi-phase Chan and Vese [2] (`CV2LS`), N-level sets with energy-based coupling by Zhang *et al.,* [3] (`ZZNLS`), and our novel four-color level sets with energy-based and explicit topological coupling [6] (`NBP4LS-ETC`). The latter two techniques use coupling constraints in order to prevent the merging of adjacent cells when they approach or touch each other.

– `CV2LS`: In order to segment multiple (i.e., N distinct) objects, Vese and Chan extended their previous 2-phase algorithm [1] by using $\lceil \log_2 N \rceil$ level sets [2]. The corresponding energy functional $E_{pc}(\boldsymbol{c}, \Phi)$

$$E_{pc}(\mathbf{c}, \mathbf{\Phi}) = \sum_{1 \le i \le N} \mu_i \int_{\mathbf{\Omega}(\boldsymbol{y})} (\boldsymbol{I}(\boldsymbol{y}) - c_i)^2 \, \chi_i \, d\boldsymbol{y} + \sum_{1 \le i \le \lceil \log_2 N \rceil} \nu_i \int_{\mathbf{\Omega}(\boldsymbol{y})} |\nabla H(\phi_i)| \, d\boldsymbol{y}$$

where, N is the number of phases (i.e., regions in the image) associated with $\lceil \log_2 N \rceil$ level set functions, $\boldsymbol{I}$ is the gray-level image being segmented, $\mathbf{\Phi}$ is a

vector of level set functions, $\mathbf{c}$ is a vector of mean gray-level values (i.e., $c_i = mean(\boldsymbol{I})$ in the class i), χ_i is the characteristic function for each class i formed by associated Heaviside functions $H(\phi_i)$, and (μ_i, ν_i) are constants associated with the energy and length terms of the functional, respectively.

The $\lceil \log_2 N \rceil$ level set formulation improves on the performance of a single level set function, as more number of objects with varying intensities can be efficiently classified. But does not prevent under-segmentation (i.e. incorrect merges), when the objects have similar intensities (i.e. cells).

– `ZZNLS`: To overcome the drawbacks of classical Chan and Vese level set formulations, while at the same time solving the problem of apparent merging of cells during tracking, Zhang *et al.,* [3] proposed a new model using $N-$level sets for segmenting cells. Here N is the number of cells at a given time instance. An *a priori* knowledge that cells do not merge during the evolution process was used to guide the segmentation process. This was achieved by a pair-wise energy-based coupling constraint on the level sets evolution process. A similar formulation was used by Dufor *et al.,* in 3D cell segmentation [4].

The energy functional, $E_{nls}(\boldsymbol{c_{in}}, c_{out}, \boldsymbol{\Phi})$, used to solve the evolution of $N-$level sets is given by [3]:

$$E_{nls}(\boldsymbol{c_{in}}, c_{out}, \boldsymbol{\Phi}) = \gamma \sum_{i=1}^{N} \sum_{j=i+1}^{N} \int_{\boldsymbol{\Omega}} H(\phi_i) H(\phi_j)\, d\boldsymbol{y} + \nu \sum_{i=1}^{N} \int_{\boldsymbol{\Omega}} |\nabla H(\phi_i)|\, d\boldsymbol{y}$$
$$+ \mu_{in} \sum_{i=1}^{N} \int_{\boldsymbol{\Omega}} (I - c_{in}^{i})^2\, H(\phi_i)\, d\boldsymbol{y} + \mu_{out} \int_{\boldsymbol{\Omega}} (I - c_{out})^2 \prod_{\substack{i=1 \\ \forall\, i: H(\phi_i) < 0}}^{N} \Big(1 - H(\phi_i)\Big)\, d\boldsymbol{y} \tag{1}$$

Here, $\boldsymbol{\Phi} = [\phi_{i:\, i=1 \ldots N}]$ represents $N-$level sets associated with N cells in the image; $\boldsymbol{c_{in}}$ represents average intensities of cells for $H(\phi_i) \geq 0$ while c_{out} is the average intensity of the background[1]. The first term of the functional penalizes pair-wise couplings between level sets, while the second term controls the length of ϕ_i. $\mu_{in}, \mu_{out}, \gamma, \nu$ are constants associated with the functional.

– `NBP4LS-ETC`: The $N-$level set formulation described previously is able to overcome the apparent merging of neighboring cells. However this approach is not very scalable and is computationally expensive since for N objects it requires $N^2/2$ couplings. To overcome the computational cost, while still preventing the incorrect merges, we propose an *optimized* version of the $N-$level set algorithm described previously.

Our optimization is based on the fact that only neighboring cells can potentially merge. Through Delaunay triangulation the cell-to-cell neighborhood relationships are identified and represented in a graph where vertices represent the cells and edges represent the neighborhood relations.

The four-color theorem [7, 8, 9] states that any planar graph is four-colorable such that no two neighboring vertices have the same color. Thus, four rather than

[1] The region *exterior to all level sets* indicates the background.

$N-$ level sets would suffice to classify $N-$objects (i.e., cells) in an image while insuring that neighboring objects do not share the same level set.

In order to evolve the four level sets we propose minimizing an energy functional, $E_{fc}(\boldsymbol{c_{in}}, c_{out}, \boldsymbol{\Phi})$, shown in Eq. 2. The first two terms of the right-hand side of Eq. 2 are used to compute average intensities ($\boldsymbol{c_{in}}, c_{out}$) within each level set, and outside all level sets, respectively. Using an *a priori* assumption that all the foreground objects (i.e., cells) in the image have very similar characteristics, we use a single average intensity c_{in} (i.e., $\forall\, i,\ c_{in}^i = c_{in}$). Whereas Zhang *et al.,* model of computing average intensities for each cell (Eq. 2). The third term helps in minimizing the length of all level sets; the fourth term is the energy-based coupling constraint, used previously, in Eq. 2. The last term enforces the constraint of $|\nabla\phi_i| = 1$, thus helping us avoid explicit redistancing of level sets during the evolution process [10]. Regularized Heaviside and Dirac-delta functions, proposed by Chan and Vese in [1], are also used in our energy functional. $\mu_{in}, \mu_{out}, \nu, \gamma, \eta$ are constants associated with the functional.

$$E_{fc}(\boldsymbol{c_{in}}, c_{out}, \boldsymbol{\Phi}) = \mu_{in}\Big\{\sum_{i=1}^{4}\int_{\boldsymbol{\Omega}}(I - c_{in}^i)^2\, H(\phi_i)\Big\}\, d\boldsymbol{y} +$$

$$\mu_{out}\int_{\boldsymbol{\Omega}}(I - c_{out})^2 \prod_{\substack{i=1 \\ \forall\, i: H(\phi_i)<0}}^{4}\Big(1 - H(\phi_i)\Big)\, d\boldsymbol{y} + \nu\Big\{\sum_{i=1}^{4}\int_{\boldsymbol{\Omega}}|\nabla H(\phi_i)|\, d\boldsymbol{y}\Big\} +$$

$$\gamma\sum_{i=1}^{4}\sum_{j=i+1}^{4}\int_{\boldsymbol{\Omega}} H(\phi_i)H(\phi_j)\, d\boldsymbol{y} + \eta\Big\{\sum_{i=1}^{4}\int_{\boldsymbol{\Omega}}\frac{1}{2}(|\nabla\phi_i| - 1)^2\, d\boldsymbol{y}\Big\} \qquad (2)$$

The four Euler-Lagrange evolution equations associated with the minimization of Eq. 2 are as follows ($i = 1, 2, 3, 4$):

$$\frac{\partial\phi_i}{\partial t} = \delta(\phi_i)\Bigg\{\mu_{in}(I - c_{in}^i)^2 - \mu_{out}(I - c_{out})^2 \prod_{\substack{j=1 \\ \forall\, j: H(\phi_j)<0, j\neq i}}^{4}\Big(1 - H(\phi_j)\Big)$$

$$- \nu\,\mathrm{div}\Big(\frac{\nabla\phi_i}{|\nabla\phi_i|}\Big) + \gamma\sum_{j=1; j\neq i}^{4} H(\phi_j)\Bigg\} + \eta\Bigg\{\Delta\,\phi_i - \mathrm{div}\Big(\frac{\nabla\phi_i}{|\nabla\phi_i|}\Big)\Bigg\} \qquad (3)$$

where, Δ is the Laplacian operator.

In addition to the energy-based coupling technique of ZZNLS [3] to penalize overlaps between level sets, we use an explicit topological coupling technique. First, we compute $\delta(\phi_i); i \in [1, 4]$. As we use a narrow-band approach (i.e., $\delta(\phi_i) > s_{thresh}$) to update the level set curves we check the saliency of $\delta(\phi_i)$ i.e., $\delta(\phi_i) > \delta(\phi_j); j \neq i$. This helps us identify pixels on the front of the current level set that may lie on narrow-band fronts of other level sets. A pixel on the front of a current level set is updated only if this saliency test is satisfied. If however a "collision" is detected between cells, then the evolution of level sets near the "collision" region stops. To speed up convergence as in [11] and [12] we use level set segmentation from a previous frame as an initial estimate for a current frame.

For details on implementing the four-level set algorithm, we direct the reader to [6].

3 Multiple Cell Tracking Using Correspondence Graphs

Tracking is a fundamental step in the analysis of long term behavior of migrating cells. In this section we present a detection based cell tracking algorithm that extends our previous work in [13]. Tracking is done by resolving frame to frame correspondences between multiple cells segmented using active contour level set methods as described in Sec.2.

3.1 Summary of Tracking Algorithm

1. For each frame $I(\boldsymbol{y}, t)$ at time t, the tracking module receives four foreground mask layers, $\Omega_{\mathrm{k}}(\mathrm{t})$, that correspond to level sets from the "four-color" segmentation algorithm. In order to refine cell boundaries and remove spurious regions, morphological operations (e.g., opening, closing) *may* be performed on these foreground layers.
2. Connected component analysis is performed on all refined foreground layers such that each $\Omega_{\mathrm{k}}(\mathrm{t})$ is partitioned into n_k disjoint regions

$$\Omega_{\mathrm{k}}(\mathrm{t}) = \{\Omega_{\mathrm{k},1}(\mathrm{t}), \Omega_{\mathrm{k},2}(\mathrm{t}), \ldots, \Omega_{\mathrm{k},\mathrm{n_k}}(\mathrm{t})\}$$

   that ideally correspond to n_k individual cells.
3. For each disjoint region $\Omega_{\mathrm{k,i}}$, features such as bounding box, centroid, area, and support map are extracted. Region information from all four layers are combined and relabeled as

$$\Omega_{\mathrm{i}}(t),\ \mathrm{i} \in [1 \ldots n],\ \text{ and } \ n = \sum_{k=1}^{4} n_k$$

   without merging connected regions from different foreground layers. Keeping regions from different foreground layers distinct, even when they are spatially connected, preserves the identities of previously disjoint cells, thus preventing false trajectory merges.
4. Relabeled region information is arranged in an "`Object-Match`" graph structure $\mathcal{O}_{\mathcal{GR}}$ that is used in tracking (Fig. **??**). Nodes in the graph represent objects $\Omega_{\mathrm{i}}(\mathrm{t})$, while edges represent object correspondences.
5. Correspondence analysis searches for potential object (cell) matches in consecutive frames. $\mathcal{O}_{\mathcal{GR}}$ is updated by linking nodes corresponding to objects in frame $I(\boldsymbol{y}, t)$ with nodes of potential corresponding objects in frame $I(\boldsymbol{y}, t-1)$. The confidence value $\mathcal{C}_{\mathcal{M}}(i, j)$ for each match is stored with each link. This is explained further in the following sub-section.
6. The trajectory generation and validation module analyses the $\mathcal{O}_{\mathcal{GR}}$ graph and generates valid cell trajectories.

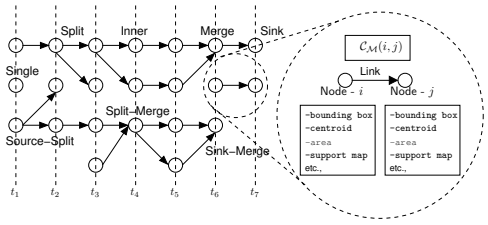

Fig. 1. An Object-Match graph structure, OGR used in cell tracking. Nodes represent detected cells and associated cell features, while links represent frame-to-frame cell correspondences and associated match confidence values.

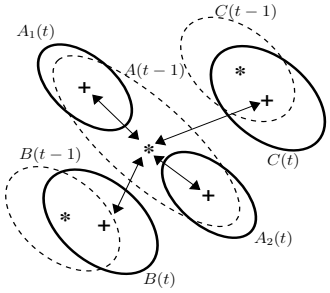

Fig. 2. Centroid distances during cell division. Cell A at time $t-1$ divides into cells A_1 and A_2 at time t. Centroid distances from the parent A to its children $\overline{AA_1}$ and $\overline{AA_2}$ are comparable in magnitude to centroid distances to its neighbors $\overline{AB}$ and $\overline{AC}$ resulting in ambiguities.

3.2 Cell-to-Cell Correspondence

Cell-to-cell matching (correspondence) is performed using a multi-stage overlap distance $\mathcal{D}_{\mathcal{MOD}}$, which consists of three distinct distance functions $\mathcal{D}_{\mathcal{BBX}}$, $\mathcal{D}_{\mathcal{MSK}}$, and $\mathcal{D}_{\mathcal{OLP}}$ for three different ranges of cell motion.

– The *inter-bounding-box distance* $\mathcal{D}_{\mathcal{BBX}}$ quantifies the long-range displacement between two regions (cells) in consecutive frames, by the distance between their bounding boxes defined as the minimum Euclidean distance between corner pairs of the two bounding boxes.

Let $\mathbf{\Lambda}[\mathcal{BBX}(\Omega_{\mathrm{i}}(\mathrm{t})), k]$ and $\mathbf{\Lambda}[\mathcal{BBX}(\Omega_{\mathrm{j}}(\mathrm{t\text{-}1})), l]$, indicate the k^{th} and l^{th} corners of the bounding box covering $\Omega_{\mathrm{i}}(\mathrm{t})$ and $\Omega_{\mathrm{j}}(\mathrm{t\text{-}1})$. $\mathcal{D}_{\mathcal{BBX}}$ can then be defined as

$$\mathcal{D}_{\mathcal{BBX}}(\Omega_{\mathrm{i}}, \Omega_{\mathrm{j}}) = \eta_b \min_{k,l} \left\{ \left|\left| \mathbf{\Lambda}[\mathcal{BBX}(\Omega_{\mathrm{i}}), k] - \mathbf{\Lambda}[\mathcal{BBX}(\Omega_{\mathrm{j}}), l] \right|\right| \right\} \tag{4}$$

where, η_b is a constant.

– The *inter-mask distance* $\mathcal{D}_{\mathcal{MSK}}$ quantifies the mid-range displacement between two regions (cells) in consecutive frames, by the minimum contour to contour distance. This distance is computed in terms of the minimum number of dilations needed to overlap the two regions as

$$\mathcal{D}_{\mathcal{MSK}}(\Omega_{\mathrm{i}}, \Omega_{\mathrm{j}}) = \eta_m \underset{\min_k}{\arg} \left\{ (\, \Omega_{\mathrm{i}} \oplus_k s_I) \cap \Omega_{\mathrm{j}} \neq 0 \right\} \tag{5}$$

where, $\oplus_k$ denotes k-times dilation, s_I denotes unit structuring element, and η_m is a constant.

– The *tonal-weighted overlap distance* $\mathcal{D}_{\mathcal{OLP}}$ quantifies the small-range displacement between two regions (cells) by the degree of their overlap, in terms of shape *and* tonal dissimilarities. In order to emphasize overlap in nuclei (i.e., dark regions with low intensity values), and to de-emphasize cytoplasm overlap (i.e., light regions with high intensity values), overlapping and non-overlapping regions are weighted by local tonal differences between two regions as

$$\mathcal{D}_{\mathcal{OLP}}(\Omega_{\mathrm{i}},\Omega_{\mathrm{j}}) = \eta_o \Big\{ \int_{\Omega_{\mathrm{i}} \setminus \Omega_{\mathrm{j}}} (1 - I_i(\boldsymbol{y}))\, d\boldsymbol{y} \; + \int_{\Omega_{\mathrm{j}} \setminus \Omega_{\mathrm{i}}} (1 - I_j(\boldsymbol{y}))\, d\boldsymbol{y} + \int_{\Omega_{\mathrm{i}} \cap \Omega_{\mathrm{j}}} |I_i(\boldsymbol{y}) - I_j(\boldsymbol{y})|\, d\boldsymbol{y} \Big\} \Big/ \Big\{ \int_{\Omega_{\mathrm{i}}} I_i(\boldsymbol{y}) d\boldsymbol{y} + \int_{\Omega_{\mathrm{j}}} I_j(\boldsymbol{y}) d\boldsymbol{y} \Big\} \quad (6)$$

where, the intensity images $I_i(\boldsymbol{y}) = I_i(\boldsymbol{y}, t)$ and $I_j(\boldsymbol{y}) = I_j(\boldsymbol{y}, t-1)$, and are scaled such that $I \in [0, 1]$. η_o is a constant. The first two terms in the numerator of Eq. 6 account for the distance due to uncovered regions in frames at time instants t and $t-1$, respectively. The complement of intensity images are used to obtain higher distances for uncovered low intensity regions (i.e., nuclei). The third term in the numerator accounts for the intensity dissimilarity within the overlapping region. The denominator is used to normalize the distance by the area of the two cells being compared.

$\mathcal{D}_{\mathcal{MOD}}$ can be assigned any of the three distance measures described above, as per the following rules,

$$\mathcal{D}_{\mathcal{MOD}}(\Omega_{\mathrm{i}},\Omega_{\mathrm{j}}) = \begin{cases} \mathcal{D}_{\mathcal{BBX}} & \text{if} \quad \mathcal{BBX}(\Omega_{\mathrm{i}}) \cap \mathcal{BBX}(\Omega_{\mathrm{j}}) = \emptyset \\ \mathcal{D}_{\mathcal{MSK}} & \text{if} \quad \Omega_{\mathrm{i}} \cap \Omega_{\mathrm{j}} = \emptyset \\ \mathcal{D}_{\mathcal{OLP}} & \text{otherwise} \end{cases} \quad (7)$$

The proposed multi-stage distance measure depends on size and shape similarity of the compared regions, besides their proximity, and thus have several advantages over the widely used centroid distance measure.

A particularly important case for cell tracking is *mitosis* (i.e., cell division). During mitosis, epithelial cells often become elongated, subsequently splitting across the minor axis. This produces a big increase in the centroid distance and the distances between a cell and its children become comparable to the distances between a cell and its neighboring cells (Fig. 2). In such a scenario, a low gating threshold would result in parent-to-children matches being discarded, resulting in discontinuities in cell trajectories. However, if a high gating threshold is used, correspondence ambiguities may arise. The proposed multi-stage overlap distance measure overcomes these problems.
In addition to object separation based measures, shape (contour) similarity metrics can also be added to the distances described above as additional matching criteria. Since for cell tracking we are primarily interested in the displacement parameter, those metrics are not used in this study but they will be considered in future.

During tracking a match matrix $\overline{\overline{\mathcal{M}}}$ and a confidence matrix $\overline{\overline{\mathcal{C}_{\mathcal{M}}}}$ for each frame, $I(\boldsymbol{y}, t)$, are produced. $\mathcal{M}(\Omega_{\mathrm{i}},\Omega_{\mathrm{j}})$ indicates whether the i^{th} object in $I(\boldsymbol{y}, t)$, corresponds to the j^{th} object in $I(\boldsymbol{y}, t-1)$. $\mathcal{C}_{\mathcal{M}}(\Omega_{\mathrm{i}},\Omega_{\mathrm{j}})$ indicates the confidence of this match and consist of two components,

– *Similarity confidence*, $\mathcal{C}_{\mathcal{SIM}}(\Omega_{\mathrm{i}}, \Omega_{\mathrm{j}})$, is a measure of the similarity between the matched objects and is defined as

$$\mathcal{C}_{\mathcal{SIM}}(\Omega_{\mathrm{i}}, \Omega_{\mathrm{j}}) = 1 - \frac{\mathcal{D}_{\mathcal{MOD}}(\Omega_{\mathrm{i}}, \Omega_{\mathrm{j}})}{\mathcal{D}^{\max}_{\mathcal{MOD}}} \tag{8}$$

where, $\mathcal{D}^{\max}_{\mathcal{MOD}}$ is a user defined constant used to normalize $\mathcal{D}_{\mathcal{MOD}}$.

– *Separation confidence*, $\mathcal{C}_{\mathcal{SEP}}(\Omega_{\mathrm{i}}, \Omega_{\mathrm{j}})$, measures the competition between possible matches for the current object and is defined as

$$\mathcal{C}_{\mathcal{SEP}}(\Omega_{\mathrm{i}}, \Omega_{\mathrm{j}}) = \begin{cases} 1 & \text{no competitor,} \\ 0.5\left\{1 - \dfrac{\left(\mathcal{D}_{\mathcal{MOD}}(\Omega_{\mathrm{i}},\Omega_{\mathrm{j}}) - \mathcal{D}_{\mathcal{MOD}}(\Omega_{\mathrm{i}},\Omega^{*}_{\mathrm{j}})\right)}{\max\left(\mathcal{D}_{\mathcal{MOD}}(\Omega_{\mathrm{i}},\Omega_{\mathrm{j}}), \mathcal{D}_{\mathcal{MOD}}(\Omega_{\mathrm{i}},\Omega^{*}_{\mathrm{j}})\right)}\right\} & \text{otherwise} \end{cases} \tag{9}$$

where, Ω_{j} indicates the current candidate being compared with Ω_{i}, and Ω_{j^*} is its closest competitor in terms of distance. This measure favors matches without competitors, and matches with competitors having higher distances.

Unfeasible correspondences are eliminated using confidence values. Absolute pruning eliminates matches whose confidence values are below a certain threshold, while relative pruning eliminates matches whose confidence values are below a percentage of the confidence for the best match.

3.3 Trajectory Generation and Validation

Trajectory segments are generated from $\mathcal{O}_{\mathcal{GR}}$ using a multi-hypothesis testing approach with delayed decision. Besides one-to-one object matches, the proposed tracking algorithm supports many-to-one, one-to-many, many-to-many, one-to-none, or none-to-one matches that may result from false detections or associations, segmentation errors, occlusion, entering, exiting, or division of cells.

The segment generation module analyzes match information by classifying the nodes of $\mathcal{O}_{\mathcal{GR}}$ (cells) into nine types; *s*ingle, source, source-split, sink, inner, split, sink-merge, merge-split, merge, based on the number of parent and child objects.

A data structure (`Segment-List`) is formed by identifying and organizing a linked list (`Trajectory-Segments`) of inner objects starting with a source or split type cell and ending with a merge or sink type cell. Extracted segments are labeled using a method similar to connected component labeling.

Not all the detected segments correspond to actual cell trajectories. Trajectory validation unit checks the validity of each segment based on criteria such as duration, length, linearity, size of the corresponding object, parent and children segments etc. and filters out invalid segments. Trajectories are formed by linking unfiltered segments sharing the same label. Discontinuity resolution is also done in this unit using Kalman filter prediction.

4 Results and Analysis

The proposed cell segmentation and tracking system has been tested on a wound healing image sequence consisting of 136 frames of dimensions 300×300 (40μm×40μm)

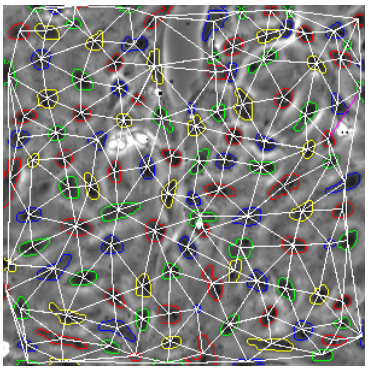

Fig. 3. Segmentation mask obtained using our four-level set formulation with an explicit topological coupling constraint and the associated Delaunay graph for frame #136

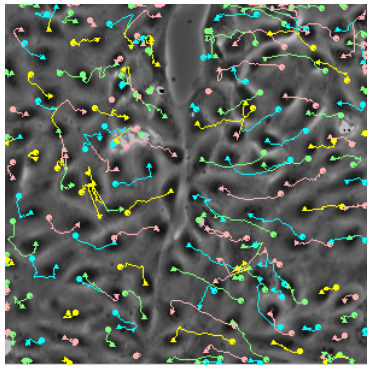

Fig. 4. Trajectories obtained using the described tracking algorithm on masks from our four-level set formulation with an explicit topological coupling constraint

Table 1. Tracking results, when using three different segmentation algorithms. The number of frames in the sequence = 136, with dimensions of each frame equal to 300×300.

	R-P	T-O	T-S	T-M	T-A	T-D
CV2LS	85%	16748	44	16	14	23
NBP4LS-EC	85%	16732	33	2	29	33
NBP4LS-ETC	85%	17161	22	0	25	20

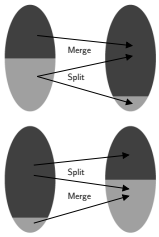

Fig. 5. False splits and merges that result from fragmentation in cells

with image intensities $I \in [0, 255]$. The sequence has been obtained using a monolayer of cultured pig epithelial cells, as described by Salaycik *et al.,* in [14]. Images were sampled uniformly over a 9:00:48 hour period and acquired using a phase contrast microscope, with a 10× objective lens, and at a resolution of approximately 0.13μm per pixel.

Three segmentation algorithms have been implemented: a multi-phase Chan and Vese level set algorithm (CV2LS); our four-level set algorithm with only energy-based coupling (NBP4LS-EC); and our four-level set algorithm with energy-based and explicit topological coupling NBP4LS-ETC. The tracking algorithm described in Sec. 3 has been applied to the three sets of masks obtained from these segmentation algorithms, and the results have been compared. For all three segmentation algorithms the following parameters have been used: $\mu_{in} = 1, \mu_{out} = 1, \nu = 1.0/(255.0)^2$ and the number of iterations for each frame has been set to a fixed number $K = 15$. For the

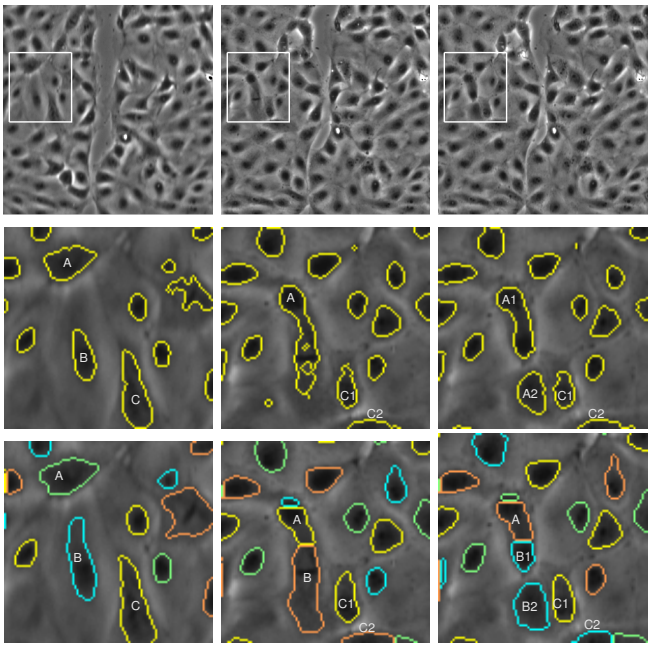

Fig. 6. Evolution of three cells labelled as A,B, and C. First row: Original frames #78,#103, and #111. Second and third rows: segmentation results for CV2LS and NBP4LS-ETC algorithms respectively. Segmentation results are zoomed to the region of interest ([70,10]-[170,110]) marked on the original frames. In row 3, contour colors associated with each object are changing from frame to frame due to re-coloring of the neighborhood graph in order to reflect changes in the neighborhood relationships.

segmentation algorithms with energy-based coupling constraint γ has been set to 0.1. During tracking, a relative pruning rate of 85% has been used and matches with confidence values below 85% of $\mathcal{C}_{\mathcal{BST}}$ have been pruned. ($\mathcal{C}_{\mathcal{BST}}$ indicates the confidence of the best match for the current object). The tracking results have been filtered by object size and segment length. Size threshold T_{os} has been set to 30 pixels, and duration threshold T_{sl} has been set to 5 frames. Incomplete objects at the image borders (i.e., within 20 pixels from each side) have been excluded from the statistics.

Representative results for our segmentation (NBP4LS-ETC) and tracking algorithms are given in Figures 3 and 4. Figure 3 shows segmented cells and their neighborhood relationships in the form of a Delaunay graph. Figure 4 shows the cell trajectories obtained after tracking. Table 1 shows tracking results obtained using the tracking algorithm described in Section 3, on masks produced by three different segmentation algorithms, CV2LS, NBP4LS-EC and NBP4LS-ETC. **T-O** indicates the total number of disjoint objects (i.e., cells) detected in all frames of the image sequence. **T-S** indicates the number of trajectory segments that split from another trajectory segment. Such splits may result from cell division, or fragmentation during segmentation. **T-M** indicates number of trajectory segments that merge with other trajectory segments. **T-A** and **T-D** indicate numbers of trajectory segments that appear or disappear, unexpect-

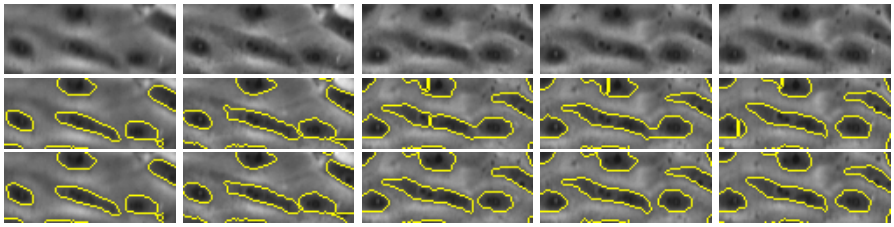

Fig. 7. Segmentation results for the frames #72, #79, #110, #113 and #118, zoomed to the region of interest ([256,13]-[295,110]). First row: original sequence. Second row: segmentation using NBP4LS-EC algorithm. Third row: segmentation using NBP4LS-ETC algorithm (contours shown without level set color).

edly. These may occur when no evidence of cells in the current frame exists in previous frames, or when no match exists in future frames for cells present in the current frame. The NBP4LS-ETC algorithm does a better job than either the NBP4LS-EC or the CV2LS algorithm in preventing false-merges of cells. Fragmentation is a problem with both the NBP4LS-ETC and NBP4LS-EC algorithms. But as shown in Table 1, the NBP4LS-ETC results in a smaller number of splits than either NBP4LS-EC or CV2LS algorithms. As shown in Fig. 5, false splits and merges may arise when a cell is fragmented in the current frame, or becomes fragmented in a future frame. Proposed method removes fragments at the image level through post-processing of small objects using morphology and at the trajectory level through filtering short segments.

Figures 6 and 7 show two cases that demonstrate the advantage of our NBP4LS-ETC method. Figure 6 shows the evolution of three cells labeled as A,B, and C. In the sequence from frame #78 to #111 two of the cells undergo mitosis (cell division). Cell C divides first followed by B; between frames #78 and #103 cell C splits into children cells C1 and C2; between frames #103 and #111 cell B splits into children cells B1 and B2. Both algorithms CV2LS (2^{nd} row), and NBP4LS-ETC (3^{rd} row) correctly identify the mitosis event of cell C. But only NBP4LS-ETC correctly identifies the mitosis event of cell B. Using the CV2LS method, at frame #103 cell B that is clearly distinct in frame #78, gets falsely merged with cell A, because cell B becomes indistinct (the nucleus is not as thick as preparation for DNA replication) and at the same time the region between cells A and B gets darker as these cells move closer together. This false merge causes additional tracking complications when cell B undergoes subsequent mitosis. As seen in frame #111, cell A appears to undergo mitosis and is incorrectly associated with the children A1 and A2. Cell A2 is associated with parent cell A instead of parent B due to a correspondence error; it should be labeled as cell B2. Object A1 is associated with parent object A due to both correspondence and segmentation errors; the segmentation of object A1 merges two actual cells (labeled A and B1 in row 3) which leads to the association error during tracking. However using the NBP4LS-ETC algorithm the explicit topological coupling constraint prevents cells A and B from merging and the mitosis of cell B is correctly detected and tracked. Effects of fragmentation such as the small region above cell A in frames #103 and #111 are handled by postprocessing and trajectory filtering and did not cause any tracking errors.

Figure 7 depicts an “absorption event” where one level set pushes a neighboring

level set out of its own path of evolution. Using only an energy-based coupling term (2^{nd} row - `NBP4LS-EC`) leads to the shifting of the boundary between adjacent objects. Ultimately one object " absorbs" the other without a merge event (where adjacent level sets merge together during contour evolution). Using the proposed additional explicit topological coupling term as described, the location of the boundary is maintained which prevents absorption. The absorption process may be order dependent but we have found that randomization of level set processing order is not sufficient to prevent absorption.

5 Conclusion

We have presented an automated cell segmentation and tracking system designed to study migration of cells imaged with a phase contrast microscope. Cells that move into the field-of-view, arise from cell division or disappear due to apoptosis are reliably segmented and tracked by this system. The novel four-color level set formulation introduced to deal with the false-merge problem in segmentation and tracking of dense cell clusters, is very scalable and significantly reduces the computational complexity of $N-$level set formulation of Zhang *et al.,* [3]. Experimental results show that segmentation with the proposed four-level set formulation, with an explicit topological coupling constraint, greatly improves accuracy of trajectories obtained during cell tracking. Further research on trajectory validation and behavior analysis is currently in progress.

References

1. T.Chan, L.Vese: Active contours without edges. *IEEE Trans. Image Process.* **10** (2001) 266–277
2. L.Vese, T.Chan: A multiphase level set framework for image segmentation using the Mumford and Shah model. *Intern. J. Comput. Vis.* **50** (2002) 271–293
3. B.Zhang, C.Zimmer, J.-C.Olivo-Marin: Tracking fluorescent cells with coupled geometric active contours. In: *Proc. 2^{nd} IEEE Int. Symp. Biomed. Imaging (ISBI)*, Arlington, VA (2004) 476–479
4. A.Dufour, V.Shinin, S.Tajbakhsh, N.Guillén-Aghion, J.-C.Olivo-Marin, C.Zimmer: Segmenting and tracking fluorescent cells in dynamic 3-D microscopy with coupled active surfaces. *IEEE Trans. Image Process.* **14** (2005) 1396–1410
5. C.Zimmer, J.-C.Olivo-Marin: Coupled parametric active contours. *IEEE Trans. Pattern Anal. Machine Intell.* **27** (2005) 1838–1842
6. S.Nath, K.Palaniappan, F.Bunyak: Cell segmentation using coupled level sets and graph-vertex coloring. In R.Larsen and M.Nielsen and J.Sporring, ed.: *LNCS - Proc. MICCAI 2006*. Springer-Verlag (2006)
7. K.Appel, W.Haken: Every planar map is four colorable. Part I. discharging. *Illinois. J. Math.* **21** (1977) 429–490
8. K.Appel, W.Haken, J.Koch: Every planar map is four colorable. Part II. reducibility. *Illinois. J. Math.* **21** (1977) 491–567
9. N.Robertson, D.P.Sanders, P.D.Seymour, R.Thomas: The four color theorem. *J. Combin. Theory, Ser. B* **70** (1997) 2–44
10. C.Li, C.Xu, C.Gui, D.Fox: Level set evolution without re-initialization: A new variational formulation. In: *Proc. IEEE Conf. Computer Vision Pattern Recognition*. Volume 1. (2005) 430–436

11. D.P.Mukherjee, N.Ray, S.T.Acton: Level set analysis for leukocyte detection and tracking. *IEEE Trans. Image Process.* **13** (2001) 562–672
12. N.Paragiois, R.Deriche: Geodesic active contours and level sets for the detection and tracking of moving objects. *IEEE Trans. Pattern Anal. Machine Intell.* **22** (2000) 266–280
13. F.Bunyak, K.Palaniappan, S.K.Nath, T.I.Baskin, G.Dong: Quantitive cell motility for *in vitro* wound healing using level set-based active contour tracking. In: *Proc. 3^{rd} IEEE Int. Symp. Biomed. Imaging (ISBI)*, Arlington, VA (2006)
14. K.J.Salaycik, C.J.Fagerstrom, K.Murthy, U.S.Tulu, P.Wadsworth: Quantification of microtubule nucleation growth and dynamics in wound-edge cells. *J. Cell Sci.* **118** (2005) 4113–4122